JACS
JOURNAL OF THE AMERICAN CHEMICAL SOCIETY
Communication
pubs.acs.org/JACS

Pt Nanoparticles@Photoactive Metal–Organic Frameworks: Efficient Hydrogen Evolution via Synergistic Photoexcitation and Electron Injection

Cheng Wang, Kathryn E. deKrafft, and Wenbin Lin*

Department of Chemistry, CB#3290, University of North Carolina, Chapel Hill, North Carolina 27599, United States

Supporting Information

ABSTRACT: Pt nanoparticles of 2–3 nm and 5–6 nm in diameter were loaded into stable, porous, and phosphorescent metal–organic frameworks (MOFs **1** and **2**) built from $[Ir(ppy)_2(bpy)]^+$-derived dicarboxylate ligands ($\mathbf{L_1}$ and $\mathbf{L_2}$) and $Zr_6(\mu_3\text{-}O)_4(\mu_3\text{-}OH)_4(carboxylate)_{12}$ secondary building units, via MOF-mediated photoreduction of K_2PtCl_4. The resulting Pt@MOF assemblies serve as effective photocatalysts for hydrogen evolution by synergistic photoexcitation of the MOF frameworks and electron injection into the Pt nanoparticles. Pt@**2** gave a turnover number of 7000, approximately five times the value afforded by the homogeneous control, and could be readily recycled and reused.

Metal–organic frameworks (MOFs) have emerged as an interesting class of porous crystalline materials that can be easily functionalized at the molecular level.[1] The coexistence of intrinsic porosity and functionality enables their applications in a variety of fields such as gas storage and separation,[2] drug delivery,[3] bioimaging,[4] chemical sensing,[5] and catalysis.[6] Functional entities can be built into MOF frameworks (walls) either as bridging ligands[7] or as secondary building units (SBUs).[8] They can also be tethered onto MOF walls via postsynthetic modifications.[9] Functional entities can also be assembled inside the internal channels or cavities of MOFs as counterions or as trapped nanoparticles (NPs).[10] In particular, metal NPs have been incorporated into MOFs through chemical vapor deposition,[11] liquid/incipient wetness impregnation,[12] solid grinding,[13] and microwave irradiation[14] to form metal@MOF hierarchical assemblies. Such a versatile variety of functionalization methods makes it possible to incorporate multiple functional entities into the same MOF to enable synergistic functions.[15]

We are interested in using photoactive framework materials as a new platform to integrate different functional components that are needed for solar energy conversion.[16] Photocatalytic hydrogen generation is an essential half reaction in water splitting, which converts sunlight energy into the chemical potential of hydrogen molecules.[17] A visible light-driven photocatalytic hydrogen evolution system often requires two components—the phosphor to harvest sunlight and the catalyst to produce hydrogen using the harvested energy. Bernhard et al. pioneered the use of $[Ir(ppy)_2(bpy)]^+$ (ppy = 2-phenylpyridine; bpy = 2,2′-bipyridine) and its derivatives as photosensitizers to drive photocatalytic hydrogen evolution with Pt NPs.[18] We report here the design of synergistic hydrogen evolution photocatalysts based on Pt NP@MOF assemblies. Pt NPs were loaded into the cavities of phosphorescent MOFs (**1** and **2**) to enable efficient photocatalytic H_2 evolution via photoinjection of electrons from the light-harvesting MOF frameworks into the Pt NPs. The Pt@**2** assembly showed a much enhanced (~five times) hydrogen evolution efficiency compared to the homogeneous control and could be readily recycled and reused by centrifugation.

The $[Ir(ppy)_2(bpy)]Cl$-derived dicarboxylic acids $H_2\mathbf{L_1}$ and $H_2\mathbf{L_2}$ were synthesized by treating $[Ir(ppy)_2Cl]_2$ with diethyl (2,2′-bipyridine)-5,5′-dicarboxylate ($Et_2\mathbf{L_1}$) and dimethyl (2,2′-bipyridine)-5,5′-dibenzoate ($Me_2\mathbf{L_2}$), respectively, followed by base-catalyzed hydrolysis (Supporting Information [SI]).[16a] We targeted the synthesis of UiO frameworks built from a linear dicarboxylate ligand and the $Zr_6(\mu_3\text{-}O)_4(\mu_3\text{-}OH)_4(carboxylate)_{12}$ SBU in this work because of their high chemical stability.[19] As reported previously,[16a] $Zr_6(\mu_3\text{-}O)_4(\mu_3\text{-}OH)_4(bpdc)_{5.94}(\mathbf{L_1})_{0.06}$ (MOF-**1**) was prepared by doping the $\mathbf{L_1}$ ligand into the UiO-67 framework with biphenyldicarboxylate (BPDC) as the bridging ligand at ~2 wt % loadings, by taking advantage of the matching length of $\mathbf{L_1}$ and BPDC (Scheme 1). Intergrown octahedral nanocrystals of **1** of ~200 nm in dimensions (Figure 2a) were used for hydrogen evolution studies. **1** is highly porous with a BET surface area of 1194 m^2/g and an average pore size of 6.7 Å (SI).

MOF-**2** was synthesized by treating $H_2\mathbf{L_2}$ with $ZrCl_4$ in DMF at 100 °C for 3 days. Cuboctahedron-shaped single crystals of **2**, approximately 0.02 mm in each dimension, were obtained and used for X-ray diffraction studies.[20] **2** adopts the UiO framework structure of the **fcu** topology by connecting the $Zr_6(\mu_3\text{-}O)_4(\mu_3\text{-}OH)_4(carboxylate)_{12}$ SBUs with the linear $\mathbf{L_2}$ linker (Figure 1a,b). Because of the steric bulk of the $\mathbf{L_2}$ ligand, a noninterpenetrated structure was obtained, with a 71.4% void space as calculated by PLATON and a triangular open channel with a 1.6 nm edge length and an octahedral cavity with a diameter of 1 nm. The disordered nature of the solvent molecules and counterions in the MOF channels prevents their identification by X-ray crystallography. The solvent molecules and counterions were instead determined by a combination of TGA and NMR studies (SI), which gave the overall formula of $Zr_6(\mu_3\text{-}O)_4(\mu_3\text{-}OH)_4(\mathbf{L_2})_6\cdot 64DMF$ for **2**. Nitrogen adsorption measurements on **2** indicated zero surface area. Powder X-ray

Received: January 17, 2012
Published: April 9, 2012

dx.doi.org/10.1021/ja300539p | J. Am. Chem. Soc. 2012, 134, 7211–7214

Scheme 1. Synthesis of Phosphorescent Zr-Carboxylate MOFs (1 and 2) of the fcu Topology and Subsequent Loading of Pt NPs inside MOF Cavities via MOF-Mediated Photoreduction of K_2PtCl_4 to Form the Pt@1 and Pt@2 Assemblies

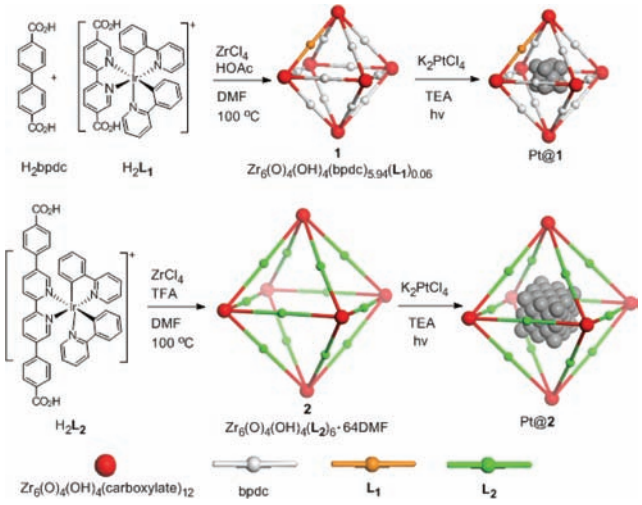

diffraction (PXRD) studies indicated severe framework distortion for **2** upon solvent removal (SI), a process that is common for MOFs with large open channels.[21] The porosity of **2** was instead ascertained by dye uptake measurements. **2** exhibited an approximately 75 wt % uptake of both Brilliant Blue R-250 and Crystal Violet (SI).

The $[Ir^{III}(ppy)_2(bpy)]^+$ moiety in **1** and **2** can be excited by visible light to a ^{1}MLCT excited state, which efficiently transitions to a ^{3}MLCT state through intersystem crossing. The long-lived ^{3}MLCT state then returns to the ground state to lead to phosphorescence emission (Figure S14 inset). Time-resolved emission measurements revealed the weighted lifetime

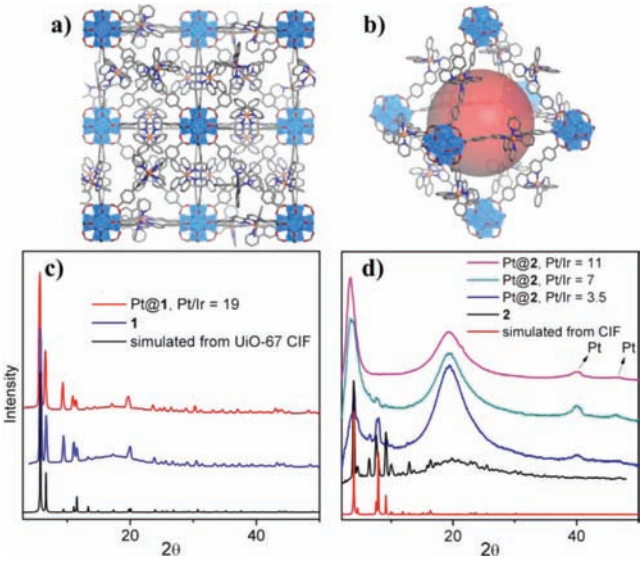

Figure 1. Stick-polyhedron model of the crystal structure of **2**, as viewed along the [100] direction (a) and showing an octahedral cavity (b), represented by a red ball with a diameter of 1 nm; PXRD patterns of (c) Pt@**1**(red), **1** (blue), the idealized UiO-67 framework (black), and (d) **2** (black), Pt@**2** with different Pt/Ir ratios (3.5, blue; 7, green; 11, purple), and the idealized framework of **2** (red).

of the ^{3}MLCT state of **1** to be 51.8 ns (vs 11.1 ns for Et_2L_1) and that of **2** to be 110.3 ns (vs 89.0 ns for Me_2L_2) (Figure S14). We believe the longer emission lifetimes of MOFs than those of corresponding ligands are due to the rigidity of the MOF frameworks.

Pt NPs were loaded into the cavities of **1** and **2** by *in situ* photoreduction of K_2PtCl_4. A mixture of K_2PtCl_4 and the MOF powder in a mixed solvent of tetrahydrofuran (THF)/triethylamine (TEA)/H_2O (20/1/1 v/v/v) was degassed by bubbling N_2 through for 10 min before being placed in front of a 450 W Xe-lamp with a 420 nm cutoff (long pass) filter. TEA can reductively quench the photoexcited $[Ir^{III}(ppy)_2(bpy)]^{+*}$ to generate the reduced radical $[Ir^{III}(ppy)_2(bpy^{\bullet-})]$ which can reduce K_2PtCl_4 to form Pt NPs in the homogeneous systems.[18] We found that K_2PtCl_4 could be photoreduced by the ultraviolet (UV) light from the Xe-lamp in the absence of Ir-phosphors via direct UV light absorption by K_2PtCl_4. We placed a 420 nm cutoff filter in front of the Xe-lamp to reliably control the formation of Pt NPs only inside MOF cavities.

The formation of Pt@MOF assemblies is supported by the following observations. Upon Pt loading, the color of the MOF powders changed from reddish-orange to brown or black due to the plasmonic absorption of Pt NPs.[22] Diffuse reflectance spectra of the Pt@MOF samples are shown in Figure 3b. Pt NPs with diameters of 2−3 nm and 5−6 nm were formed inside the cavities of **1** and **2**, respectively, as revealed by high-resolution transmission electron microscopy (HRTEM) (Figure 2). The fact that the Pt NP sizes are larger than

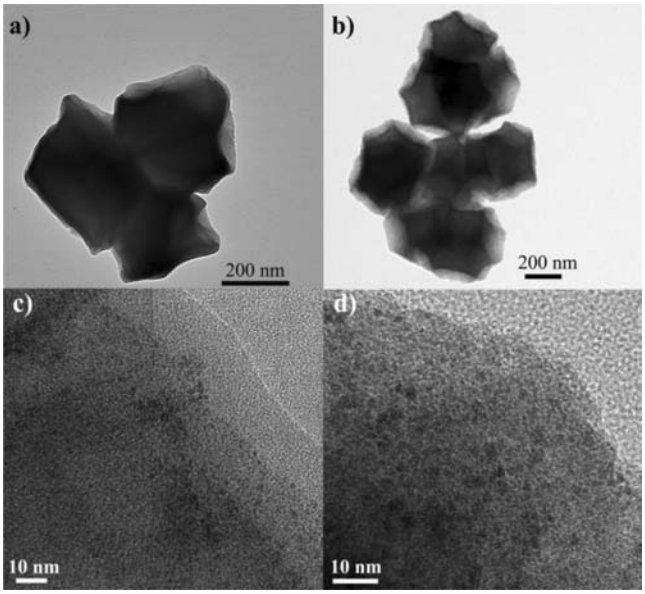

Figure 2. TEM images of Pt@**1** (a and c) and Pt@**2** (b and d). The black dots in (c) and (d) are Pt NPs.

those of the MOF cavities indicates partial MOF framework distortion/degradation during Pt NP formation; this phenomenon has been commonly observed for metal@MOFs.[11a] Energy dispersive X-ray spectroscopy (EDS) confirmed the presence of Pt in the samples (SI). The amounts of Pt NPs in the samples were quantitatively determined by inductively coupled plasma-mass spectrometry (ICP-MS). As **2** possesses a more open framework structure and contains a much higher concentration of Ir-phosphor than **1**, much higher loadings of Pt were incorporated into **2** when the same amount of K_2PtCl_4

dx.doi.org/10.1021/ja300539p | J. Am. Chem. Soc. 2012, 134, 7211−7214

was used in the reactions. The Pt@**2** samples reached a plateau Pt/Ir molar ratio of 40, corresponding to 240 Pt atoms per $Zr_6(\mu_3\text{-}O)_4(\mu_3\text{-}OH)_4(carboxylate)_{12}$ SBU and a filling of 47% of the void volume of **2**. In comparison, the Pt@**1** samples showed a maximum Pt/Ir ratio of 53 (corresponding to 3 Pt atoms per SBU). The drastically different Pt loadings in **1** and **2** correlate well with the different Ir-phosphor loadings of the two MOFs.

PXRD patterns of Pt@**1** showed that the framework structure of **1** was retained upon the loading of Pt NPs (Figure 1c). On the other hand, peaks in the PXRD patterns of Pt@**2** gradually broadened with increasing Pt loadings, indicating significant structural distortion caused by the NPs in the MOF channels (Figure 1d). Peaks due to Pt NPs at 39.7° and 46.4° also became more pronounced in the PXRD patterns as the Pt loadings increased. Different structural impacts of Pt NPs on **1** and **2** are consistent with the higher Pt loadings and larger MOF cavity/Pt NP sizes of Pt@**2** compared to those of Pt@**1**.

The *in situ* generated Pt@MOF assemblies were examined for their photocatalytic activities for hydrogen evolution using visible light (>420 nm). The $[Ir^{III}(ppy)_2(bpy^{\bullet-})]$ radicals generated by TEA-mediated photoreduction can transfer electrons to the Pt NPs to reduce protons for hydrogen production. The amounts of hydrogen generated were quantified by GC analysis of the headspace gas in the reactor using methane gas as the internal standard. The amount of K_2PtCl_4 added in the suspension was optimized for the Pt@MOFs to generate the largest amount of hydrogen in 6 h (SI). Under the optimized conditions, the Pt/Ir ratio in the MOF sample was determined by ICP-MS to be 18.6 and 17.8 for Pt@**1** and Pt@**2**, respectively. The highest hydrogen evolution turnover number (TON) for each MOF based on Ir phosphors (Ir-TON) in 6 h is 730 and 1620 for Pt@**1** and Pt@**2**, respectively. The assembled Pt@MOFs can be recovered from the solution by centrifugation after the reaction and used again for hydrogen evolution in a fresh solution without adding additional K_2PtCl_4. The Ir-TONs of the recovered catalysts are only slightly lower than those of the first run (Table 1). The

Table 1. Pt@MOFs as Photocatalyst for Hydrogen Evolution[a]

entry	catalyst	Ir-TON[b]	Pt-TON
1	Pt@**1** (1st run)	730	39.2
2	Pt@**1** (2nd run)	633	34.0
3	Pt@**1** (3rd run)	624	33.5
4	Pt@**1** (4th run)	740	39.8
5	Pt@**2** (1st run)	1620	90.9
6	Pt@**2** (2nd run)	1500	84.1
7	Pt@**2** (3rd run)	990	55.6
8	Pt@**2** (4th run)	1380	77.5

[a]Hydrogen evolution reactions were carried out for 6 h using a 450 W Xe-lamp with a 420 nm cutoff filter. [b]Ir-based turnover number (Ir-TON) is defined as $n(1/2H_2)/n(Ir)$.

catalysts could be recycled and reused at least three times. ICP-MS analysis of the supernatant solution in the second reaction run of the recovered Pt@**2** sample showed only 2.0% of the Ir and 0.5% of the Pt leaching into the solution during the run. A control experiment without addition of the MOF or K_2PtCl_4 in the solution showed no hydrogen evolution under the same experimental conditions (SI), although K_2PtCl_4 solution alone under UV light did exhibit very modest photocatalytic activity for hydrogen production (SI). TEA also proved to be a necessary sacrificial reductant in the reaction (SI), and the absence of hydrogen in the headspace of the reaction in the dark confirmed the photocatalytic nature of the reaction (SI).

To determine the total turnover number of the Pt@MOFs, time-dependent hydrogen evolution experiments were carried out over 48 h. As shown in Figure 3d, Pt@**1** and Pt@**2** samples

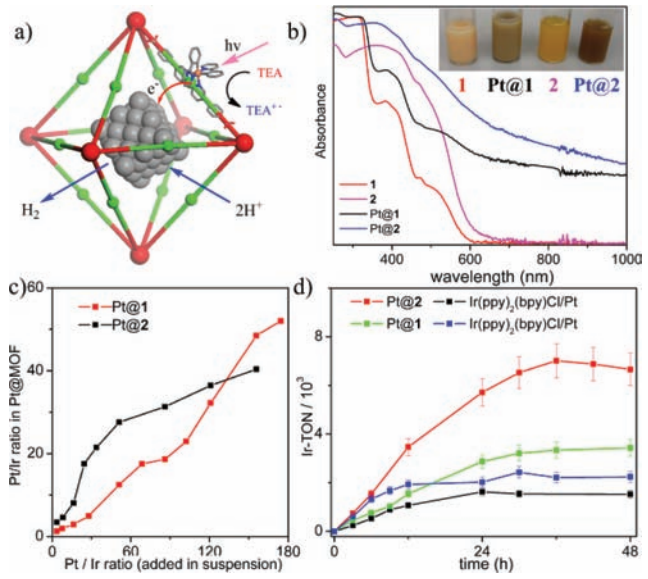

Figure 3. (a) Scheme showing the synergistic photocatalytic hydrogen evolution process via photoinjection of electrons from the light-harvesting MOF frameworks into the Pt NPs. The red balls represent $Zr_6(O)_4(OH)_4(carboxylate)_{12}$ cores, while the green balls represent the Ir-phosphor ligand of the MOF. (b) Diffuse reflectance spectra of **1** (red), Pt@ **1** (black), **2** (purple), and Pt@**2** (blue). A photograph of suspensions of these samples is shown in the inset. (c) Relationship between the amount of K_2PtCl_4 added in the reaction solution and the amount of Pt deposited inside the MOF (normalized to the amount of) for Pt@**1** (red) and Pt@**2** (black). (d) Time-dependent hydrogen evolution curves of Pt@**1** (green), Pt@2 (red), and homogeneous control $[Ir(ppy)_2(bpy)]Cl/K_2PtCl_4$ (blue and black for different Pt/Ir ratios) under optimized conditions (Pt/Ir ratios in solution/suspension for Pt@**1** and its homogeneous control is 86.0; Pt/Ir ratios in solution/suspension for Pt@**2** and its homogeneous control is 24.2; stirring rate for all reactions was 1000 rpm).

gave a total Ir-TON of 3400 and 7000, respectively. These Ir-TONs are 1.5 and 4.7 times the values afforded by the homogeneous controls $[Ir(ppy)_2(bpy)]Cl/K_2PtCl_4$ under their respective conditions (2200 and 1500, respectively). We believe that the enhanced photocatalytic hydrogen evolution activities of Pt@MOFs are due to more efficient electron transfer from the unstable $[Ir^{III}(ppy)_2(bpy^{\bullet-})]$ species to Pt NPs which not only increased hydrogen reduction rates but also slowed down the decomposition of the Ir complexes. ICP-MS of the supernatant solution of the Pt@**2**-catalyzed reaction after 48 h showed that 25.6% of the Ir leached into the solution, indicating the decomposition of the Ir-complex during the 48 h reaction. The photochemical quantum yield of the Pt@**2**-catalyzed reaction driven with 440 nm light was determined to be $(5.6 \pm 0.4) \times 10^{-4}$, much higher than that of the homogeneous control $[(3.0 \pm 0.4) \times 10^{-4}$, SI].

In summary, we have successfully loaded Pt NPs into the cavities of two stable, porous, phosphorescent UiO MOFs built from Ir-phosphor-derived linear dicarboxylate linkers and $Zr_6(\mu_3\text{-}O)_4(\mu_3\text{-}OH)_4(carboxylate)_{12}$ SBUs. The Pt@MOF

dx.doi.org/10.1021/ja300539p | J. Am. Chem. Soc. 2012, 134, 7211−7214

assemblies serve as highly efficient photocatalysts for hydrogen evolution with both higher turnover frequencies and higher turnover numbers than those of the homogeneous analogs, as a result of facile electron transfer from the photoreduced Ir phosphor to the entrapped Pt NPs. MOFs thus provide a versatile and tunable platform to hierarchically integrate different functional components for solar energy utilization.

■ ASSOCIATED CONTENT

Supporting Information

Experimental procedures and characterization data. This material is available free of charge via the Internet at http://pubs.acs.org.

■ AUTHOR INFORMATION

Corresponding Author

wlin@unc.edu

Notes

The authors declare no competing financial interest.

■ ACKNOWLEDGMENTS

This material is based upon work supported as part of the UNC EFRC: Center for Solar Fuels, an Energy Frontier Research Center funded by the U.S. Department of Energy, Office of Science, Office of Basic Energy Sciences under Award Number DE-SC0001011 (for supporting K.E.d.). C.W. acknowledges NSF-DMR and UNC Chemistry Department for an Ernest L. Eliel fellowship, and K.E.d. acknowledges the UNC Graduate School for a Dissertation Completion Fellowship. We thank Dr. A. S. Kumbhar for help with HRTEM studies.

■ REFERENCES

(1) (a) Ferey, G.; Mellot-Draznieks, C.; Serre, C.; Millange, F. *Acc. Chem. Res.* **2005**, *38*, 217. (b) Kitagawa, S.; Kitaura, R.; Noro, S. *Angew. Chem., Int. Ed.* **2004**, *43*, 2334. (c) Evans, O. R.; Lin, W. *Acc. Chem. Res.* **2002**, *35*, 511. (d) Farha, O. K.; Hupp, J. T. *Acc. Chem. Res.* **2010**, *43*, 1166.

(2) (a) Dinca, M.; Long, J. R. *Angew. Chem., Int. Ed.* **2008**, *47*, 6766. (b) Rowsell, J. L.; Yaghi, O. M. *Angew. Chem., Int. Ed.* **2005**, *44*, 4670.

(3) (a) Lin, W.; Rieter, W. J.; Taylor, K. M. *Angew. Chem., Int. Ed.* **2009**, *48*, 650. (b) Rieter, W. J.; Pott, K. M.; Taylor, K. M.; Lin, W. *J. Am. Chem. Soc.* **2008**, *130*, 11584. (c) Horcajada, P.; et al. *Nat. Mater.* **2010**, *9*, 172.

(4) (a) deKrafft, K. E.; Xie, Z.; Cao, G.; Tran, S.; Ma, L.; Zhou, O. Z.; Lin, W. *Angew. Chem., Int. Ed.* **2009**, *48*, 9901. (b) Della Rocca, J.; Lin, W. *Eur. J. Inorg. Chem.* **2010**, 3725.

(5) (a) Allendorf, M. D.; Houk, R. J.; Andruszkiewicz, L.; Talin, A. A.; Pikarsky, J.; Choudhury, A.; Gall, K. A.; Hesketh, P. J. *J. Am. Chem. Soc.* **2008**, *130*, 14404. (b) Chen, B.; Wang, L.; Xiao, Y.; Fronczek, F. R.; Xue, M.; Cui, Y.; Qian, G. *Angew. Chem., Int. Ed.* **2009**, *48*, 500. (c) Lan, A.; Li, K.; Wu, H.; Olson, D. H.; Emge, T. J.; Ki, W.; Hong, M.; Li, J. *Angew. Chem., Int. Ed.* **2009**, *48*, 2334. (d) Xie, Z.; Ma, L.; deKrafft, K. E.; Jin, A.; Lin, W. *J. Am. Chem. Soc.* **2010**, *132*, 922.

(6) (a) Ma, L.; Falkowski, J. M.; Abney, C.; Lin, W. *Nat. Chem.* **2010**, *2*, 838. (b) Ma, L.; Abney, C.; Lin, W. *Chem. Soc. Rev.* **2009**, *38*, 1248. (c) Lee, J.; Farha, O. K.; Roberts, J.; Scheidt, K. A.; Nguyen, S. T.; Hupp, J. T. *Chem. Soc. Rev.* **2009**, *38*, 1450.

(7) Song, F.; Wang, C.; Falkowski, J. M.; Ma, L.; Lin, W. *J. Am. Chem. Soc.* **2010**, *132*, 15390.

(8) Horike, S.; Dincă, M.; Tamaki, K.; Long, J. R. *J. Am. Chem. Soc.* **2008**, *130*, 5854.

(9) (a) Wu, C.-D.; Lin, W. *Angew. Chem., Int. Ed.* **2005**, *44*, 1958. (b) Tanabe, K. K.; Cohen, S. M. *Chem. Soc. Rev.* **2011**, *40*, 498.

(10) (a) Song, J.; Luo, Z.; Britt, D. K.; Furukawa, H.; Yaghi, O. M.; Hardcastle, K. I.; Hill, C. L. *J. Am. Chem. Soc.* **2011**, *133*, 16839. (b) Meilikhov, M.; Yusenko, K.; Esken, D.; Turner, S.; Van Tendeloo, G.; Fischer, R. A. *Eur. J. Inorg. Chem.* **2010**, *2010*, 3701. (c) Jiang, H. L.; Xu, Q. *Chem. Commun.* **2011**, *47*, 3351.

(11) (a) Hermes, S.; Schröter, M.-K.; Schmid, R.; Khodeir, L.; Muhler, M.; Tissler, A.; Fischer, R. W.; Fischer, R. A. *Angew. Chem., Int. Ed.* **2005**, *44*, 6237. (b) Proch, S.; Herrmannsdörfer, J.; Kempe, R.; Kern, C.; Jess, A.; Seyfarth, L.; Senker, J. *Chem.—Eur. J.* **2008**, *14*, 8204. (c) Müller, M.; Hermes, S.; Kähler, K.; van den Berg, M. W. E.; Muhler, M.; Fischer, R. A. *Chem. Mater.* **2008**, *20*, 4576.

(12) (a) Sabo, M.; Henschel, A.; Frode, H.; Klemm, E.; Kaskel, S. *J. Mater. Chem.* **2007**, *17*, 3827. (b) Yuan, B.; Pan, Y.; Li, Y.; Yin, B.; Jiang, H. *Angew. Chem., Int. Ed.* **2010**, *49*, 4054. (c) Jiang, H. L.; Akita, T.; Ishida, T.; Haruta, M.; Xu, Q. *J. Am. Chem. Soc.* **2011**, *133*, 1304. (d) Gu, X. J.; Lu, Z. H.; Jiang, H. L.; Akita, T.; Xu, Q. *J. Am. Chem. Soc.* **2011**, *133*, 11822. (e) Moon, H. R.; Kim, J. H.; Suh, M. P. *Angew. Chem., Int. Ed.* **2005**, *44*, 1261. (f) Suh, M. P.; Moon, H. R.; Lee, E. Y.; Jang, S. Y. *J. Am. Chem. Soc.* **2006**, *128*, 4710.

(13) (a) Ishida, T.; Nagaoka, M.; Akita, T.; Haruta, M. *Chem.—Eur. J.* **2008**, *14*, 8456. (b) Jiang, H.-L.; Liu, B.; Akita, T.; Haruta, M.; Sakurai, H.; Xu, Q. *J. Am. Chem. Soc.* **2009**, *131*, 11302.

(14) El-Shall, M. S.; Abdelsayed, V.; Khder, A. E. R. S.; Hassan, H. M. A.; El-Kaderi, H. M.; Reich, T. E. *J. Mater. Chem.* **2009**, *19*, 7625.

(15) Song, F. J.; Wang, C.; Lin, W. *Chem. Commun.* **2011**, *47*, 8256.

(16) (a) Wang, C.; Xie, Z. G.; deKrafft, K. E.; Lin, W. L. *J. Am. Chem. Soc.* **2011**, *133*, 13445. (b) Kent, C. A.; Mehl, B. P.; Ma, L.; Papanikolas, J. M.; Meyer, T. J.; Lin, W. *J. Am. Chem. Soc.* **2010**, *132*, 12767. (c) Kent, C. A.; Liu, D.; Ma, L.; Papanikolas, J. M.; Meyer, T. J.; Lin, W. *J. Am. Chem. Soc.* **2011**, *133*, 12940.

(17) (a) Esswein, M. J.; Nocera, D. G. *Chem. Rev.* **2007**, *107*, 4022. (b) Dubois, M. R.; Dubois, D. L. *Acc. Chem. Res.* **2009**, *42*, 1974. (c) Hammarström, L.; Hammes-Schiffer, S. *Acc. Chem. Res.* **2009**, *42*, 1859. (d) Youngblood, W. J.; Lee, S. H.; Maeda, K.; Mallouk, T. E. *Acc. Chem. Res.* **2009**, *42*, 1966.

(18) (a) Goldsmith, J. I.; Hudson, W. R.; Lowry, M. S.; Anderson, T. H.; Bernhard, S. *J. Am. Chem. Soc.* **2005**, *127*, 7502. (b) Tinker, L. L.; McDaniel, N. D.; Curtin, P. N.; Smith, C. K.; Ireland, M. J.; Bernhard, S. *Chem.—Eur. J.* **2007**, *13*, 8726. (c) Curtin, P. N.; Tinker, L. L.; Burgess, C. M.; Cline, E. D.; Bernhard, S. *Inorg. Chem.* **2009**, *48*, 10498. (d) Metz, S.; Bernhard, S. *Chem. Commun.* **2010**, *46*, 7551. (e) DiSalle, B. F.; Bernhard, S. *J. Am. Chem. Soc.* **2011**, *133*, 11819.

(19) (a) Cavka, J. H.; Jakobsen, S.; Olsbye, U.; Guillou, N.; Lamberti, C.; Bordiga, S.; Lillerud, K. P. *J. Am. Chem. Soc.* **2008**, *130*, 13850. (b) Kandiah, M.; Nilsen, M. H.; Usseglio, S.; Jakobsen, S.; Olsbye, U.; Tilset, M.; Larabi, C.; Quadrelli, E. A.; Bonino, F.; Lillerud, K. P. *Chem. Mater.* **2010**, *22*, 6632.

(20) As a result of small crystal size, X-ray diffraction data collection only leads to a data set with the resolution of 2.1 Å.

(21) Ferey, G.; Serre, C. *Chem. Soc. Rev.* **2009**, *38*, 1380.

(22) Sun, Y.; Xia, Y. *Science* **2002**, *298*, 2176.